Applied Catalysis B: Environmental 304 (2022) 120967

Contents lists available at ScienceDirect

Applied Catalysis B: Environmental

journal homepage: www.elsevier.com/locate/apcatb

Selective photocatalytic conversion of benzyl alcohol to benzaldehyde or deoxybenzoin over ion-exchanged CdS

Sung Gyu Lee [a], Myung Jong Kang [b], Myeongkee Park [a], Ki-jeong Kim [c], Hangil Lee [d,*], Hyun Sung Kim [a,*]

[a] Department of Chemistry, Pukyong National University, Busan 48513, Republic of Korea
[b] Department of Chemistry, Gangneung-Wonju National University, Gangneung 25457, Republic of Korea
[c] Beamline Research Division, Pohang Accelerator Laboratory (PAL), Pohang 37673, Republic of Korea
[d] Department of Chemistry, Sookmyung Women's University, Seoul 04310, Republic of Korea

ARTICLE INFO

Keywords:
Heterogeneous photocatalyst
C-C coupling
Aromatic alcohol oxidation
Cadmium sulfide
Silver ion

ABSTRACT

The visible light absorbing CdS nanoparticles were partially modified with Au_2S and Ag_2S via a simple cation exchange process to prepare heterostructure photocatalysts (denoted as Au_2S@CdS and Ag_2S@CdS), which were employed for the conversion of aromatic alcohols to valued-added products, such as benzaldehyde and C-C coupling products, including deoxybenzoin and hydrobenzoin. When Au_2S@CdS was used as the photocatalyst, benzaldehyde was obtained as the main product with a selectivity of 99%, and when Ag_2S@CdS was used as the photocatalyst, deoxybenzoin was obtained as the main product with a selectivity of 95%. The critical photogenerated electron and hole transfer occurring during the photocatalytic reaction was systemically investigated by performing various control experiments and using in-situ high-resolution X-ray photoelectron spectroscopy. In addition, with the photocatalytic system proposed in this study, benzyl alcohol could be photoconverted into benzaldehyde or deoxybenzoin almost completely with high selectivity by altering the cocatalyst component via simple ion exchange.

1. Introduction

The photocatalytic conversion of aromatic alcohols to various value-added products is of high significance in chemical synthesis [1–5]. One of the major oxidation products of aromatic alcohols is benzaldehyde, which is primarily used in the synthesis of various organic compounds, ranging from pharmaceuticals to plastic additives [6–8]. Currently, benzaldehyde is produced in the laboratory through stoichiometric oxidation using toxic dichromate and permanganate agents or by the hydrolysis and consecutive chlorination of toluene in the chemical industry [9]. Other major oxidation products are C–C coupling products, including benzoin, deoxybenzoin, and hydrobenzoin, which are used as precursors for the synthesis of bioactive polymer initiators [10–14]. For instance, deoxybenzoin is industrially produced by the chlorination of phenylacetic acid using PCl_3 or $SOCl_2$, or by $AlCl_3$ catalyzed C–C coupling with benzene [15]. The catalytic transformation of benzyl alcohol is accompanied by its stoichiometric oxidation by toxic chemical additives. From the viewpoint of environmental concerns, the redox transformation of aromatic alcohols should preferably be implemented with high selectivity. Thus, the development of green oxidation processes is highly attractive [16,17].

Visible light photocatalysis has garnered considerable attention as an efficient environment-friendly route for the production of various industrially important chemicals. Heterogeneous photocatalysts have demonstrated a huge potential for reducing the energy consumption of various conversion processes and the synthesis of a wide range of organic compounds [18–22]. In addition to understanding the photocatalytic pathways, it is crucial to design and fabricate suitable heterogeneous photocatalytic systems with desired properties for aromatic alcohol photoreforming.

In particular, the visible light-driven photocatalytic conversion of benzyl alcohol to value-added chemicals over heterogeneous catalyst based on semiconductors has emerged as a sustainable and environmentally benign approach for the production of industrially important chemicals. The main product of the photocatalytic conversion of benzyl alcohol is benzaldehyde and not a specific C–C coupled product with high selectivity [23–35]. Various photocatalytic systems have been investigated for the oxidation of benzyl alcohol. However, although

* Corresponding authors.
E-mail addresses: easyscan@sookmyung.ac.kr (H. Lee), kimhs75@pknu.ac.kr (H.S. Kim).

https://doi.org/10.1016/j.apcatb.2021.120967
Received 27 September 2021; Received in revised form 17 November 2021; Accepted 24 November 2021
Available online 26 November 2021

various photocatalysts with high selectivity have been reported, most of these photocatalysts yield only benzaldehyde as the product.

Recently, a few studies have demonstrated the potential of InZnS and CdS for the photocatalytic oxidation of benzyl alcohol to produce C–C coupled products under anaerobic conditions [36–43]. For instance, InZnS with a controlled Zn/In ratio and modified CdS quantum dots are promising solar light-driven photoredox-catalysts for transforming benzyl alcohol into a mixture of C–C coupled products, such as benzoin, hydrobenzoin, and deoxybenzoin [38–41]. However, the selectivity of these photocatalysts for the formation of benzoin, hydrobenzoin, and deoxybenzoin is still low.

Therefore, it is necessary to develop photocatalytic systems for the highly selective formation of C–C coupling products. Owing to its appropriate bandgap (E_g = 2.41 eV) and visible light absorption, cadmium sulfide (CdS) is considered a promising photocatalyst for the chemical transformation of various compounds [42]. Moreover, the combinations of various types of metals or metal sulfides exhibit excellent photocatalytic activity owing to the synergistic effect of their constituents. To address these issues, different strategies have been investigated, such as the combination of CdS with metals or metal sulfides possessing adequate bandgap energies. In general, the combination of two or more semiconducting components with different band offsets into a single structure results in the formation of a potential gradient at the interface, which facilitates the transfer of photogenerated electrons (e^-) and holes (h^+) along the heterostructure. In this regard, heterojunction photocatalysts have been investigated to optimize the photoreforming of benzyl alcohol. To fabricate CdS heterostructure photocatalysts with tailored designs and compositions, cation exchange has recently been extensively investigated.

Herein, by selecting cationic species such as Ag^+ and Au^+ for decorating the co-catalyst of CdS, we successfully achieved the desired photocatalytic conversion of benzyl alcohol under visible light. The CdS heterostructure photocatalysts offered higher selectivity for the major product (benzaldehyde or deoxybenzoin as a C–C coupling product) in the photoreforming reaction of benzyl compared to the pristine CdS nanoparticles. The high selectivity of the CdS photocatalytic system for the desired photoconversion product can be explained as follows. (1) The consecutive photo-oxidization due to the enhanced photogenerated hole transfer yielded benzaldehyde, and (2) the ketyl radical coupling and consecutive redox neutral process yielded deoxybenzoin as the final C–C coupling product by enhancing the photogenerated electron transfer. Furthermore, in situ irradiated X-ray photoelectron spectroscopy (XPS) and various other control photocatalytic measurements revealed the occurrence of efficient charge transfer between CdS and the cation-exchanged metal sulfide as the co-catalyst.

2. Experimental section

2.1. Materials

Cadmium nitrate tetrahydrate [$Cd(NO_3)_2{\cdot}4H_2O$, Samchun], sodium sulfide nonahydrate [$Na_2S{\cdot}9H_2O$, Merck], silver nitrate [$AgNO_3$, Sigma-Aldrich], and gold(III) chloride hydrate [$HAuCl_4{\cdot}4H_2O$, Sigma-Aldrich] were used as received for preparing CdS nanoparticles (NPs). Benzyl alcohol, benzaldehyde, benzoin, hydrobenzoin, and deoxybenzoin were purchased from Alfa Aesar and used as received.

2.2. Synthesis of the CdS photocatalysts

We synthesized hexagonal CdS NPs according to a previously reported procedure [58]. The details of the procedure are provided in the Supplementary Materials (SI-1). The Ag_2S@CdS and Au_2S@CdS NPs were prepared using a typical cation exchange method as follows. The desired amounts of the cations (Ag^+ and Au^+) were dissolved in distilled deionized water (DDW, 1 mL). The CdS NPs were dispersed in a round bottom flask (capacity: 25 mL) containing DDW (10 mL). For each Ag^+ and Au^+ exchange reaction, the prepared cation solution was introduced into the dispersed pristine CdS solution with vigorous magnetic stirring, and the mixture was kept for 2 h. During the ion exchange process, the color of the CdS particles rapidly changed from yellow to dark yellow to brown when Ag^+ ions were used and to golden brown when Au^+ ions were used. The resulting Ag_2S@CdS and Au_2S@CdS NPs were collected using centrifugation and were washed thoroughly with DDW. The collected products were dried using vacuum pumps for evacuation.

2.3. Photocatalytic reaction

The CdS photocatalysts were used for the photocatalytic oxidation or redox reaction of benzyl alcohol. A substrate solution of 0.1 M benzyl alcohol and acetonitrile (1 mL) was prepared in a Pyrex glass tube (capacity 10 mL), and the CdS photocatalysts (5 mg) were dispersed in the substrate solution with magnetic stirring for 1 min under the dark condition. The mixture was bubbled with high purity Ar gas (99.999%) for 5 min and the tube was then air-tightened with a polytetrafluoroethylene screw cap. The glass tube reactor containing the photocatalyst mixture solution was placed at a distance of 20 cm from the blue light-emitting diodes (LEDs) (445 nm, 6 W) under magnetic stirring at ~100 rpm. The intensity of the blue LED (output power: 6 W) used in this study was measured using a calibrated optical power meter (1830-C, Newport). When the intensity was measured at a distance of 100 mm from the LED along the irradiation axis, the light intensity (I) was determined to be 10 mW/cm^2. After the reaction, the photocatalyst residues were removed by centrifugation (8000 rpm for 5 min). The supernatant solution was diluted with acetonitrile/toluene as the internal standard. The conversion yield of benzyl alcohol and the selectivity of each product were determined from the gas chromatography (GC) results (Figs. S1–S2) as follows:

$$\text{Conversion Yield}(\%) = (C_{i,BA} - C_{f,BA})/C_{i,BA} \times 100 \quad (1)$$

$$\text{Selectivity}(\%) = C_{Product}/(C_{i,BA} - C_{f,BA}) \times 100 \quad (2)$$

where $C_{i,BA}$ is the initial concentration of benzyl alcohol, and $C_{f,BA}$ is the concentration of benzyl alcohol after the reaction. $C_{Product}$ is the concentration of the product, such as the benzaldehyde and C–C coupling products (hydrobenzoin, benzoin, and deoxybenzoin), obtained after the reaction.

2.4. Instrumentation

To analyze the crystal structures of the samples, their X-ray diffraction (XRD) patterns were recorded on an X-ray diffractometer (PHILIPS/X′Pert-MPD System) equipped with an X-ray tube (40 kV, 30 mA) using Ni-filtered monochromatic Cu Kα radiation (Kα = 1.54056 A). The field-emission scanning electron microscopy (FE-SEM) images of the samples were obtained using a Schottky field-emission scanning electron microscope (7600 F, JEOL). The nitrogen adsorption isotherms of the samples were collected at 77 K using a BELsorp-Max system (BEL). A GC instrument (model 7890, Agilent Instruments) equipped with a flame ionization detector and a capillary polar column (DB-5, Agilent) was used to quantitatively determine the adsorption amounts of the reactants and products. Inductively coupled plasma optical emission spectrometry (ICP-OES) (Optima 7300 DV, Perkin Elmer) was used to quantitatively analyze the exchanged ions (Ag^+ and Au^+) on CdS.

The crystal structures, microstructures, and chemical compositions of the samples were examined by obtaining their high-resolution transmission electron microscopy (HR-TEM) images and energy dispersive X-ray spectroscopy (EDX) (SuperX) profiles on a scanning transmission electron microscope (Thermo Fisher Scientific, Themis Z 3.1) equipped with a Cs S-CORR probe corrector (80–300 kV, space resolution < 0.06 nm at 300 kV). Ultraviolet-visible (UV-Vis) diffuse reflectance measurements were performed using a Shimadzu UV-2600

UV-Vis spectrophotometer equipped with integrating spheres. The ultraviolet photoelectron (UP) spectroscopy (UPS) profiles of the samples were obtained on a Kratos Axis Ultra system at the excitation energies of 60 and 130 eV to investigate their valence band structures. The electronic structures of the samples were determined by performing high-resolution XPS (HR-XPS) measurements on an X-ray photoelectron spectroscope equipped with an electron analyzer (R2000, Gamma Data Scienta) at the 10A2 beamline at the Pohang Accelerator Laboratory. A 445 nm blue LED (6 W) (Solis High-Power LED, Thorlabs, Inc., Newton, NJ, USA) was used as the light source and placed at a distance of 25 cm from the specimens during the measurements to investigate the changes in the electron densities of the samples. The Cd 3d, S 2p, Ag 3d, and Au 4f core-level XPS profiles of the samples were obtained at the photon energies of 480, 230, 430 and 150 eV, respectively, to enhance their surface sensitivity.

The photoelectrochemical characterization such as photocurrent and electrochemical impedance spectroscopy (EIS) and fluorescence lifetime measurements are described in the Supplementary Material.

3. Results and discussion

3.1. Characterization of Ag^+- and Au^+-exchanged CdS

The pristine CdS NPs were synthesized using a previously reported solvothermal method. As can be observed from the FE-SEM images shown in Fig. 1(a), the as-obtained pristine CdS NPs showed irregular morphological features with a smooth surface and a size ranging from 40 to 100 nm. The heterogeneous silver/gold sulfides were developed on the CdS NPs using a cation exchange strategy. Here, the cadmium cations were incorporated within an intact sulfide sublattice. These cations were substituted by other cations, such as Ag^+ and Au^+. When aqueous $AgNO_3$ or AuCl was added to the aqueous suspension of the CdS NPs, the Ag^+ and Au^+ cations immediately substituted the Cd^{2+} cations on the CdS NPs to form Ag_2S and Au_2S, respectively. This can be attributed to the preferential binding of water molecules to the divalent Cd^{2+} cations over the Ag^+ and Au^+ cations [44]. The SEM images revealed that the Ag_2S(5%)@CdS and Au_2S(5%)@CdS samples retained their original morphological features and particle sizes after the cationic exchange reaction (Fig. 1(b) and 1(c), respectively). In addition, the exact amounts of the exchanged Ag^+ and Au^+ cations were determined using ICP-OES (Table S1). These amounts were consistent with the number of cations added for the exchange, confirming that the ion exchange process was complete.

The surface areas of the pristine CdS, Ag_2S(5%)@CdS, and Au_2S(5%)@CdS NPs were 32, 33, and 31 m^2g^{-1}, respectively, as calculated using the Brunauer–Emmett–Teller method (Fig. S3). This result proves that the surface area of the CdS NPs is almost unchanged even after the ion exchange process.

The XRD pattern of the pristine CdS NPs showed peaks at $2\theta = 24.8°$, 26.5°, 28.2°, 36.6°, 43.7°, 47.9°, 51.8°, 66.8°, and 75.4° corresponding to the (100), (002), (101), (110), (103), (112), and (203) planes of wurtzite (hexagonal)-type CdS, respectively, as shown in Fig. 1(d) [45]. The XRD patterns of Ag_2S(5%)@CdS and Au_2S(5%)@CdS were identical to that of the pristine CdS NPs, indicating that the crystalline structure of CdS was well-preserved during the ion exchange process. In addition, the formation of Ag_2S (5%) and Au_2S on the CdS NPs after the ion exchange process could not be confirmed from the XRD patterns owing to the small quantities of Ag_2S and Au_2S and highly dispersed small domains with a size of a few nanometers.

Fig. 2(a) shows the representative HR-TEM images of pristine CdS, Ag_2S(5%)@CdS, and Au_2S(5%)@CdS. The NPs showed lattice fringes with an interplanar spacing of ~3.61 Å, which corresponds to the (−100) plane of hexagonal CdS [45]. In particular, in case of Ag_2S(5%)@CdS and Au_2S(5%)@CdS, highly dispersed domains of Ag_2S and Au_2S with a size of a few nanometers were formed on the CdS NPs, leading to the construction of a heterojunction structure. From the HR-TEM image of Ag_2S(5%)@CdS, the D-spacing value was measured to be ~3.61 Å for the (100) plane of CdS and ~2.51 Å for the (−112) plane of Ag_2S [46]. In contrast, the HR-TEM image of Au_2S(5%)@CdS revealed that the D-spacing value for the (200) plane of CdS was ~2.29 Å, while that for the (110) plane of Au_2S was ~3.41 Å [47]. Furthermore, to analyze the elemental distribution of the Ag_2S(5%)@CdS and Au_2S(5%)@CdS samples, their high-resolution STEM-EDX elemental mappings were recorded (Fig. 2(b)), which revealed that Ag_2S and Au_2S were homogeneously distributed on the CdS NPs in Ag_2S(5%)@CdS and Au_2S(5%)@CdS, respectively.

Upon ion exchange with Ag^+ and Au^+, the color of CdS changed from yellow to dark yellow and golden red, respectively as can be observed from the photographs shown in Fig. 3(a). The optical characteristics of the pristine CdS, Ag_2S(5%)@CdS, and Au_2S(5%)@CdS NPs were

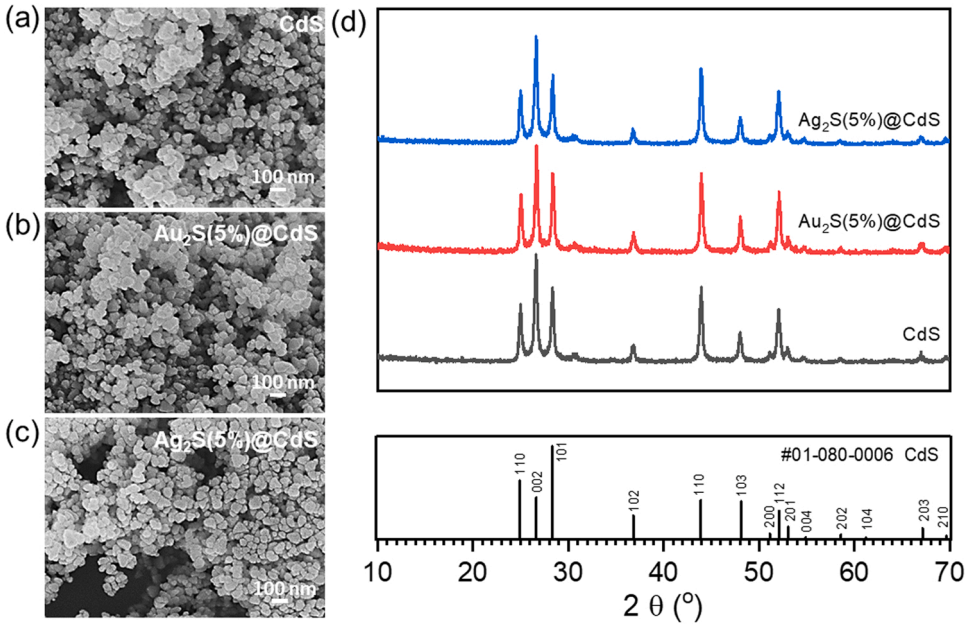

Fig. 1. SEM images of the pristine CdS (a), Au_2S(5%)CdS, (b), and Ag_2S(5%)CdS NPs (c) and their XRD patterns (d).

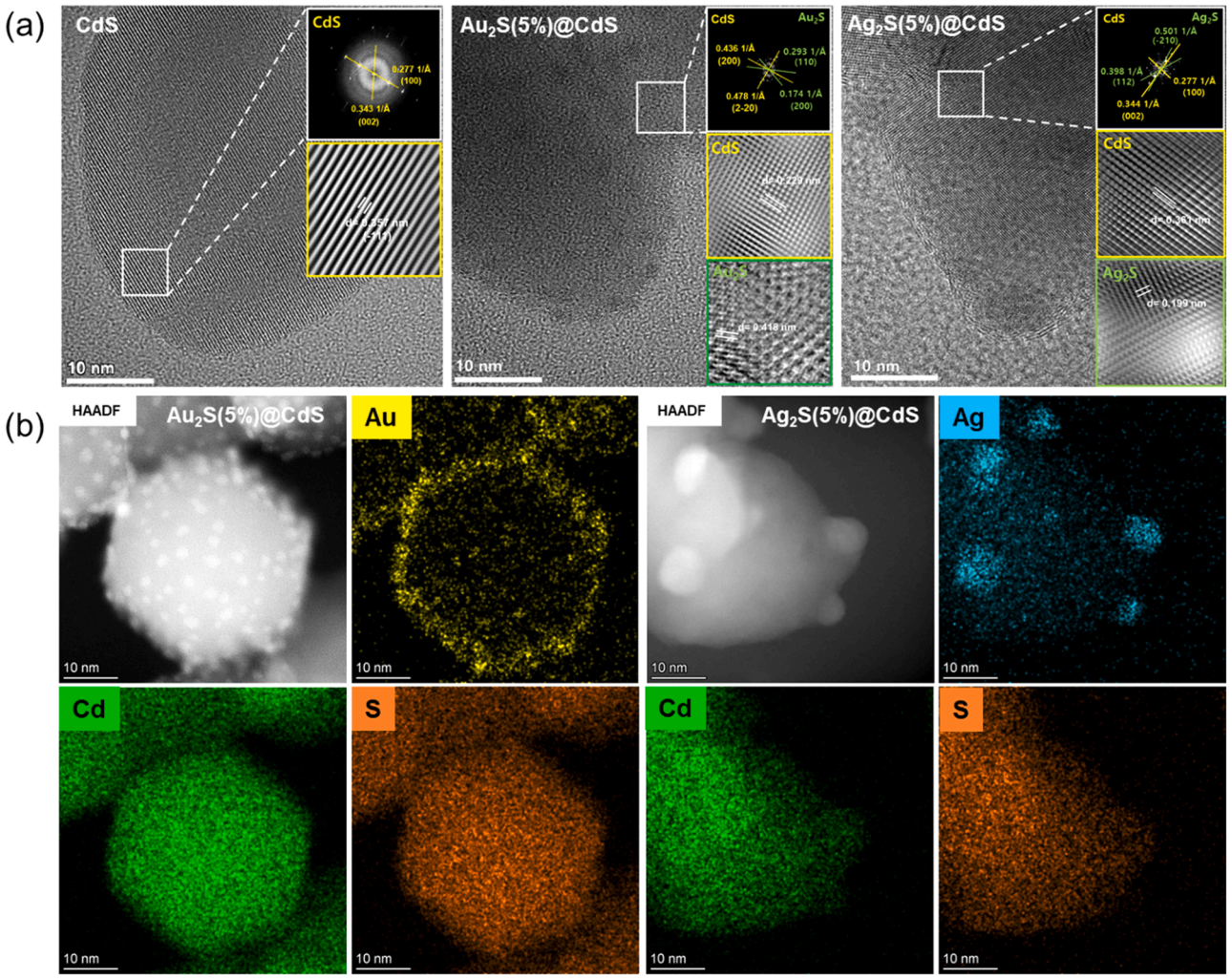

Fig. 2. HR-TEM images of the pristine CdS, Ag_2S(5%)@CdS, and Au_2S(5%)CdS NPs (a), HAADF-STEM images and corresponding elemental mappings of Au_2S(5%)@CdS and Ag_2S(5%)CdS (b).

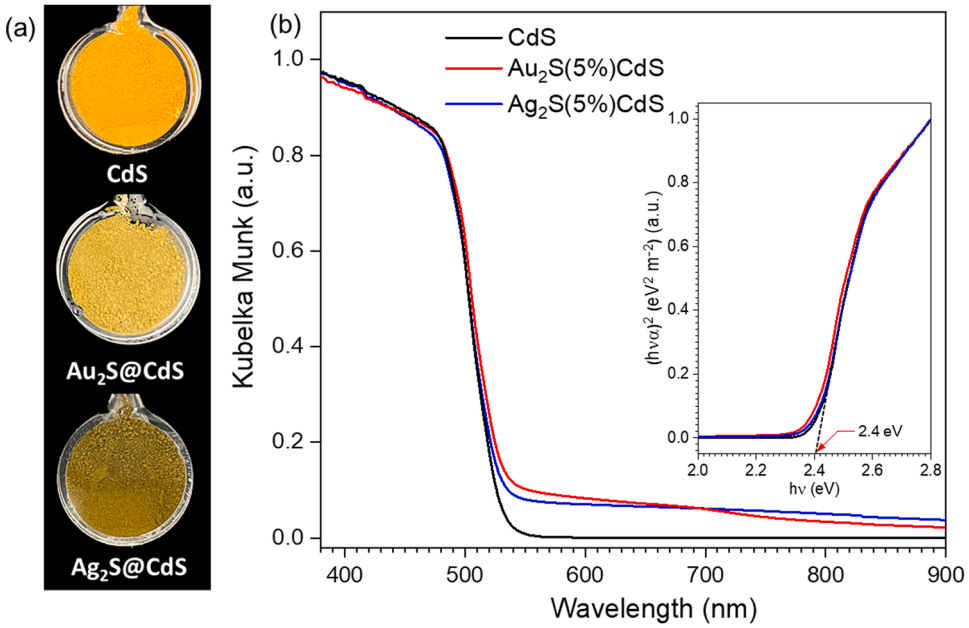

Fig. 3. Photographs (a) and diffuse reflectance UV-Vis spectra with the Tauc Plots (b) of the pristine CdS, Au_2S(5%)@CdS, and Ag_2S(5%)CdS NPs.

investigated using diffuse reflectance UV-Vis spectroscopy (Fig. 3(b)). The CdS NPs showed visible range absorption at approximately 510 nm, corresponding to the intrinsic interband electron transition in CdS. The bandgap (E_g) of pristine CdS was estimated to be 2.42 eV from its Tauc Plot obtained from the diffuse reflectance UV-Vis spectroscopy results. After the exchange process with Ag^+ and Au^+, a tailing weak absorption band appeared at wavelengths longer than 550 nm. The tailing absorption of Ag_2S(5%)@CdS and Au_2S(5%)@CdS can be attributed to the presence of small Ag_2S and Au_2S domains on the CdS surface, which were formed by the small intrinsic bandgaps of Ag_2S and Au_2S. The bandgaps (E_g) of Ag_2S(5%)@CdS and Au_2S(5%)@CdS were calculated to be 2.43 and 2.43 eV, respectively, which are similar to that of the pristine CdS NPs. This can be attributed to the formation of fine Ag_2S@CdS and Au_2S@CdS heterogeneous structures because of the preservation of the CdS lattice structure, and not the atomic-level doping of the exchange cations into the CdS lattice structure, which altered the bandgap. The as-prepared CdS-based samples exhibited strong optical absorption at approximately 450 nm, which rendered them suitable for photocatalytic reactions under the irradiation from blue LED (445 nm) as the light source.

3.2. Evaluation of photocatalytic performance

Generally, during its photocatalytic oxidation, benzyl alcohol reacts with a photogenerated hole and then undergoes deprotonation to form a ketyl radical in the anaerobic condition [39,40]. Benzaldehyde is obtained after the sequential oxidation and deprotonation of the ketyl radical, as shown in the upper part of Scheme 1. In contrast, for the C–C-coupling products, ketyl radical coupling leads to the formation of hydrobenzoin. Subsequently, hydrobenzoin can be oxidized to benzoin by the photocatalyst in a manner same as that of the oxidation of benzyl alcohol to benzaldehyde. As shown in the lower part of Scheme 1, the photocatalytic redox reaction of hydrobenzoin can yield deoxybenzoin through another route. As can be observed, three products can be obtained via C–C-coupling.

The photocatalytic oxidation of benzyl alcohol over the pristine CdS

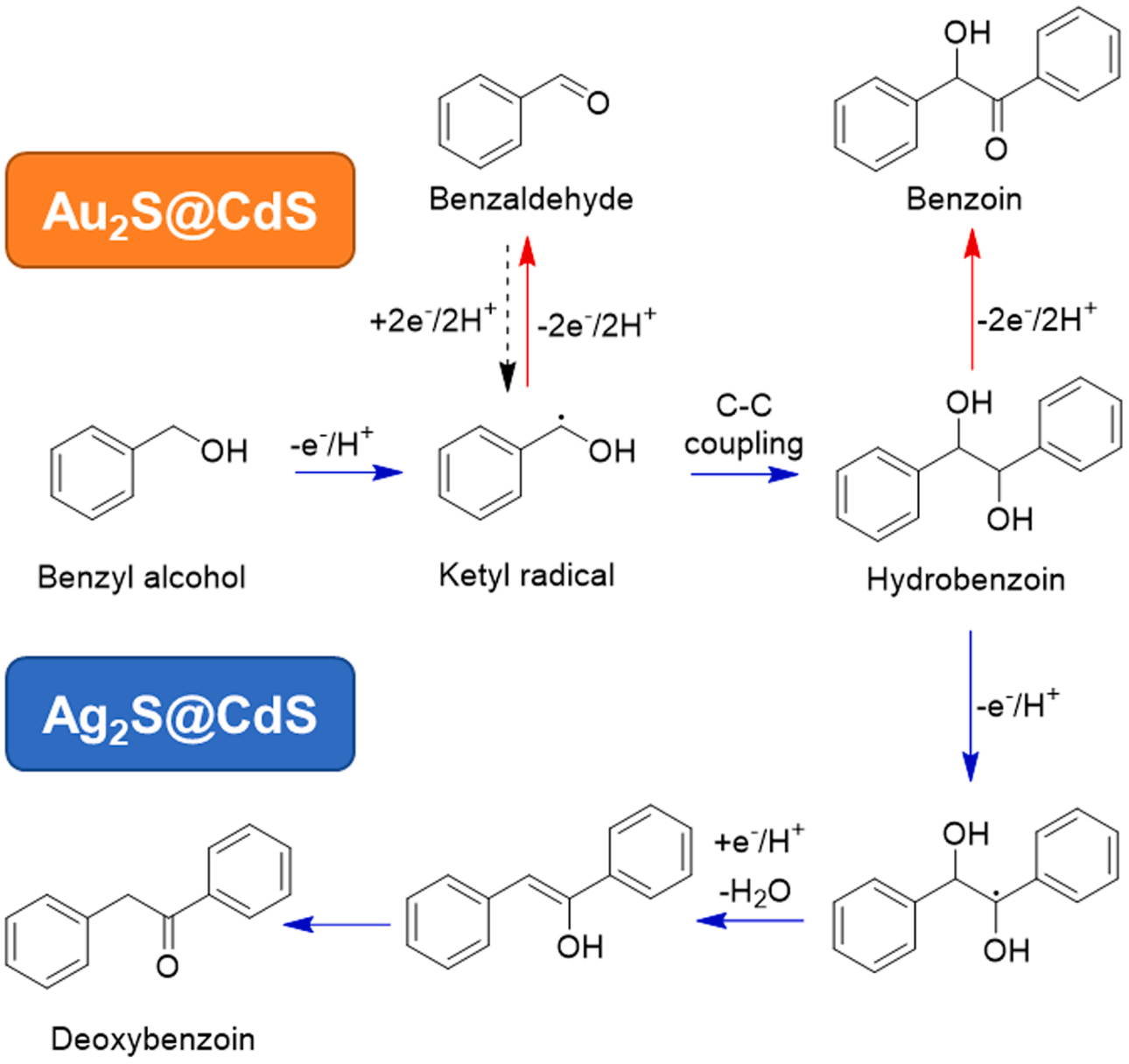

Scheme 1. Direct photocatalytic conversion route of benzyl alcohol to benzaldehyde via the photooxidation processes and C–C coupling products via the redox processes using Au_2S@CdS and Ag_2S@CdS, respectively.

NPs under blue LED light irradiation for 4 h in acetonitrile resulted in the non-selective formation of benzaldehyde and C–C coupling products (e.g. benzoin, hydrobenzoin, and deoxybenzoin). The conversion yield of the pristine CdS NPs was less than 40% with the selectivities of 34% for benzaldehyde and 65% for the C–C-coupling products, which included benzoin (15%), hydrobenzoin (27%), and deoxybenzoin (23%), as shown in Fig. 4(a). A control experiment was conducted in the absence of LED radiation. In the absence of LED irradiation, no conversion of benzyl alcohol was observed even after heating to 82 °C. In addition, the photocatalytic oxidation reaction did not occur in the absence of the CdS-based photocatalysts.

The conversion yield and selectivity of the photocatalyst toward benzaldehyde and deoxybenzoin (as the C–C coupling product) could be altered by varying the number of ions exchanged (Au^+ and Ag^+) on the CdS NPs, as shown in Fig. 4(a). Au_2S(5%)@CdS was found to be more active than the pristine CdS NPs for the photooxidation of benzyl alcohol under LED irradiation after 4 h and showed 99% conversion yield with 100% selectivity for benzaldehyde. The time profiles for Au_2S(5%)@CdS showed that its photooxidation product was only benzaldehyde (Fig. 4 (b)). In contrast, Ag_2S(5%)@CdS exhibited a significantly different activity for the photoredox reaction of benzyl alcohol under LED irradiation for 4 h. It also showed 100% conversion yield with high a selectivity of more than 95% for deoxybenzoin among the abovementioned three C–C coupling products. Interestingly, initially, deoxybenzoin and hydrobenzoin were detected with a small trace of benzaldehyde, but only deoxybenzoin was detected after 3 h of the reaction, as shown in the time profiles of the product for Ag_2S(5%)@CdS. To investigate the role of Ag_2S in inducing the reaction to increase the selectivity of Ag_2S (5%)@CdS toward deoxybenzoin, Ag_2S(x%)@CdS photocatalysts with different x values were prepared and the photoreaction was carried out under identical conditions, as shown in Fig. 4(c). When less than 2% Ag^+ ions were exchanged, the three C–C coupling products, benzoin, hydrobenzoin, and deoxybenzoin, were obtained with a low conversion yield (~40%). With an increase in the amount of exchanged Ag^+ ions, the conversion yield and selectivity toward deoxybenzoin increased. As can be observed from the reaction Scheme 1, Ag_2S induced the C–C coupling of the ketyl radical and effectively converted the first C–C coupling product i.e., hydrobenzoin to deoxybenzoin via a photoredox reaction and not to benzoin via photooxidation. In addition, the loading amount of Au_2S in Au_2S(x%)@CdS enhanced the conversion yield while maintaining the selectivity toward benzaldehyde, as shown in Fig. 4(d). These results indicate that Au_2S in Au_2S(5%)@CdS led to the sequential photooxidation of benzyl alcohol to produce benzaldehyde, while Ag_2S in Ag_2S(5%)@CdS played an important role in the prompt formation of hydrobenzoin by the generated ketyl radical and its conversion to deoxybenzoin through a photoredox reaction.

Two additional control experiments were conducted to confirm the applicability of Au_2S and Ag_2S on CdS as catalysts when excited by the blue LED (445 nm). First, the catalytic reaction was conducted upon red LED irradiation at 625 nm, which is the absorption region of Au_2S and Ag_2S, but not the CdS absorption region as seen Fig. S4. Second, Au_2S and Ag_2S NPs were separately synthesized and each photocatalytic

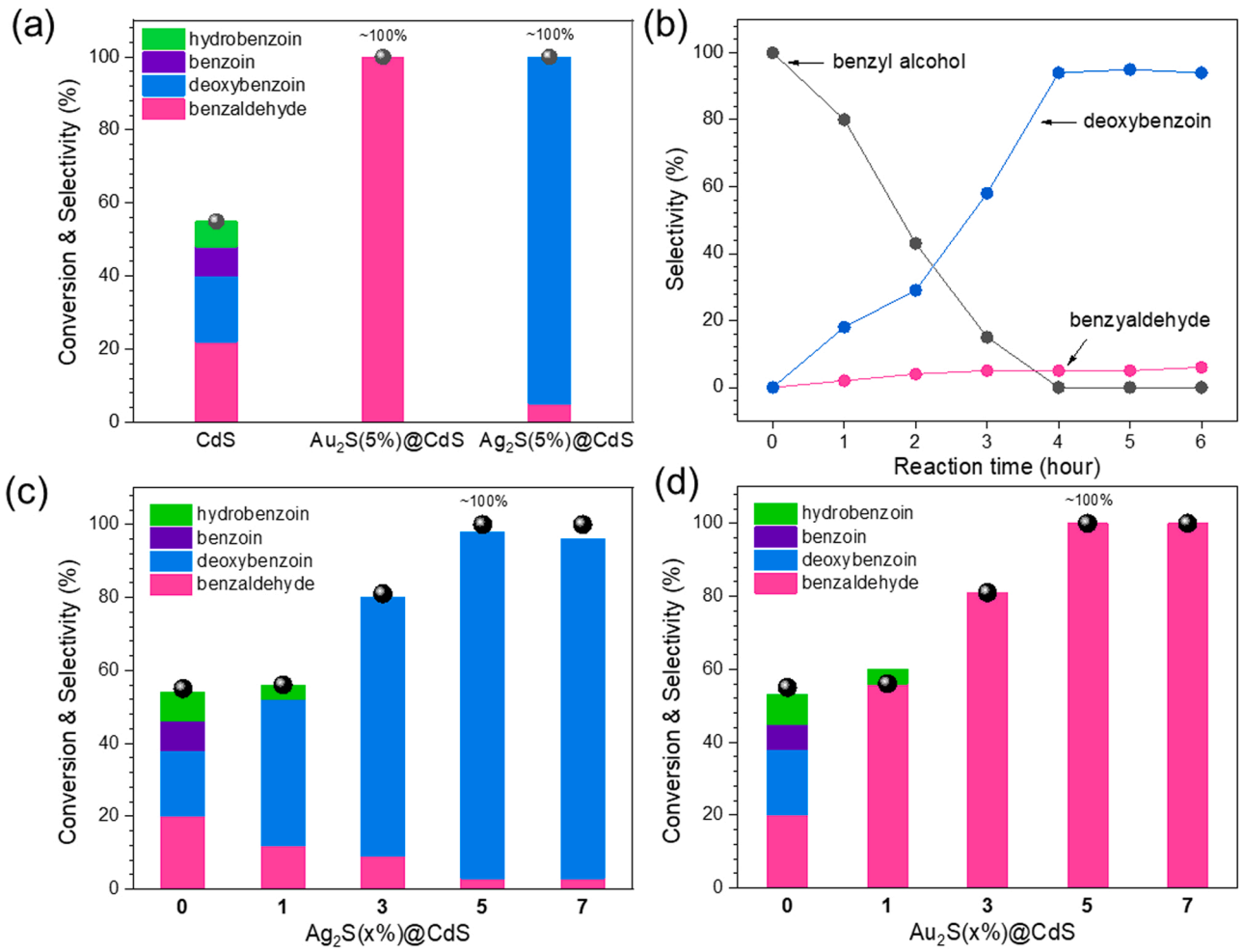

Fig. 4. Conversion and product yields of (a) pristine CdS, Au_2S(5%)CdS, and Ag_2S(5%)CdS, the variation in the reaction time of (b) Ag_2S(5%)@CdS with respect to the amounts of Ag_2S (c) and Au_2S (d) on CdS; Reaction conditions: 0.1 mmol of benzyl alcohol, 5 mg of the catalyst, 1.0 mL of CH_3CN, 4 h reaction time, Ar atmosphere, 6 W blue LEDs (445 nm) at ~35 °C.

reaction of Au_2S and Ag_2S NPs was carried out using a blue LED. In both cases, the catalytic reaction did not proceed, which suggests that Au_2S and Ag_2S on CdS serve as a co-catalyst and not a catalyst in Au_2S@CdS and Ag_2S@CdS.

To elucidate the photoredox mechanism of Ag_2S(5%)@CdS, an additional control experiment was performed using hydrobenzoin, an intermediate C–C coupling product, as a model molecule as seen Scheme 2(a). Ag_2S(5%)@CdS exhibited 100% yield during the conversion of hydrobenzoin to deoxybenzoin via the photoredox reaction under blue LED(445 nm) irradiation for 4 h. In contrast, Au_2S(5%)@CdS exhibited 100% yield during the conversion of hydrobenzoin to benzoin via photooxidation through another route. Notably, the pristine CdS NPs showed a yield of approximately 40% for the conversion of hydrobenzoin to both benzoin and deoxybenzoin, exhibiting low product selectivity. These results for the photoreaction of hydrobenzoin in the presence of Au_2S(5%)@CdS and Ag_2S(5%)@CdS were consistent with those of benzyl alcohol.

Moreover, as above mentioned about Scheme 1, the photogenerated holes lead to the oxidation of benzyl alcohol to benzaldehyde, while the photogenerated electrons are crucial for the achievement of high selectivity toward the C–C coupling products because of the presence of ketyl radicals from the back reduction of benzaldehyde. This clarifies the mechanism of the conversion of benzaldehyde or C–C coupling product from benzyl alcohol. For assessing the high selectivity of Ag_2S(5%)@CdS toward C–C coupling products, benzaldehyde was employed as a substrate in the presence of triethylamine (TEA), a hole scavenger. As seen Scheme 2(b), C–C coupling products were formed as a major product with benzyl alcohol as a minor product, indicating that ketyl radicals were consecutively reduced to form C–C coupling products such as hydrobenzoin and deoxybenzoin (conversion yield: 90%, selectivity for C–C coupling products: 99%). On the other hand, in case of the Au_2S(5%)@CdS, photocatalytic back reduction of benzaldehyde did not occurred in the presence of TEA. These results imply that Ag_2S(5%)@CdS effectively generated the photoexcited electrons to allow the formation of C–C coupling products with high selectivity. Moreover, molecular oxygen (O_2) is an electron scavenger that effectively consumes excited electrons. As demonstrated in Fig. S5, the presence of O_2 in the atmosphere completely suppressed the formation of the C–C coupling products over Ag_2S(5%)@CdS, whereas benzaldehyde was produced with relatively low conversion yield (~10%). While in case of Au_2S(5%)@CdS, although the conversion efficiency is slightly reduced to about 55% in the oxidation photoreaction under presence of O_2 in the atmosphere, the selectivity to aldehyde is still 100%. This result is consistent with the fact that excited electrons are important for the formation of C–C coupling products with high selectivity.

For verifying reusability, which is another important parameter for

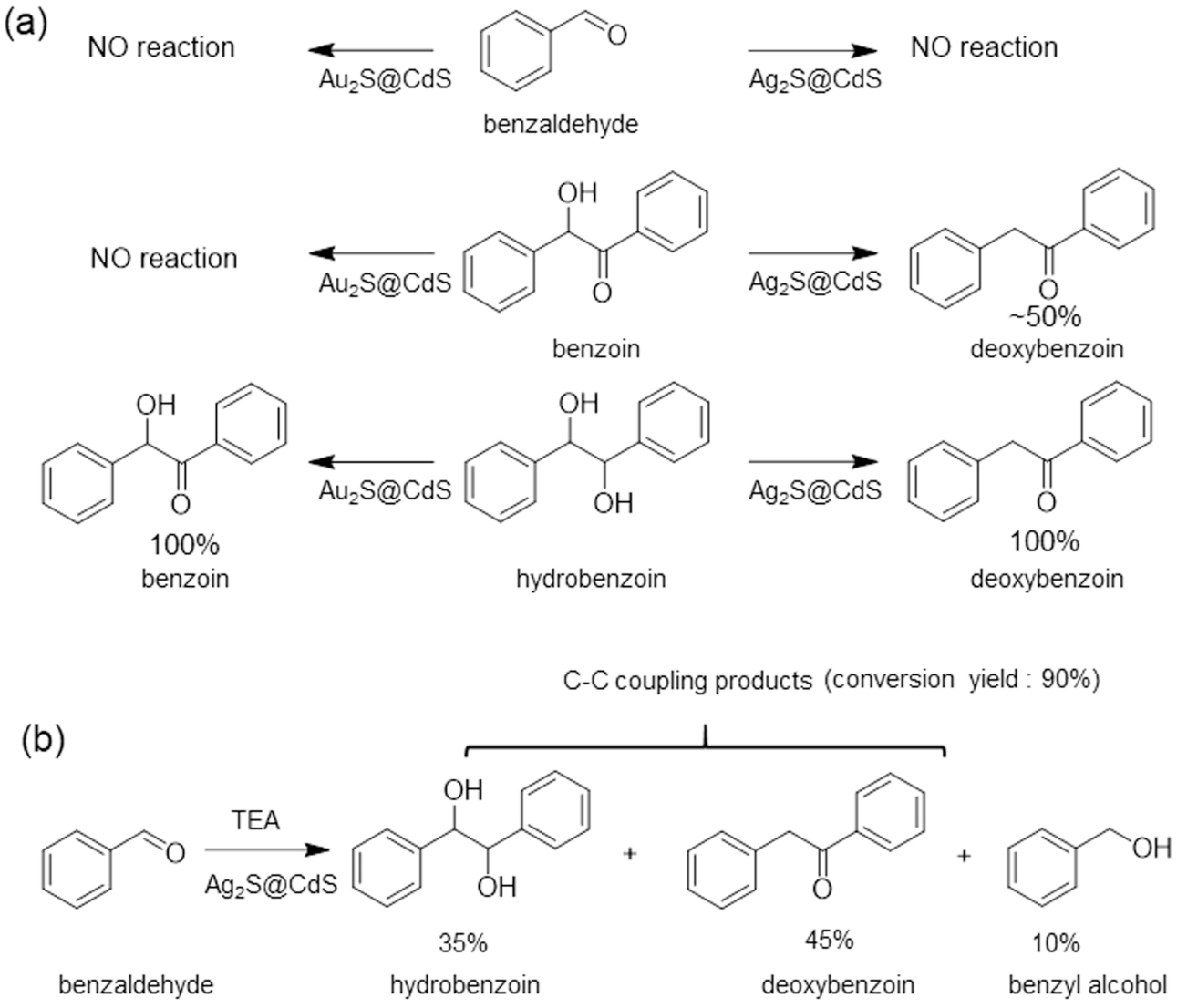

Scheme 2. Illustrations of scheme for control experiments to investigate reaction route.

estimating the photocatalytic performance, recycling experiments were conducted. As shown in Fig. S6, after three consecutive photocatalysis cycles using Au_2S(5%)@CdS and Ag_2S(5%)@CdS, the conversion yield and selectivity of catalysts were still maintained at >90% compared to those after the first cycle. Furthermore, the XRD, SEM and XPS results for recycled Au_2S(5%)@CdS and Ag_2S(5%)@CdS were identical to those for pristine samples, as seen Fig. S7. These results demonstrate the high photochemical stability of Au_2S(5%)@CdS and Ag_2S(5%)@CdS, which will broaden their practical application scope.

Moreover, the photocatalytic performance of Ag_2S(5%)@CdS was evaluated using gram-scale benzyl alcohol. We could obtain pure deoxybenzoin powder as the product in 79% yield (Fig. S8). This implies that Ag_2S@CdS composites could be applied to the scale-up of batch photochemical reactions for aromatic alcohol conversion.

3.3. Comparison with other types of photocatalysts and substrates

Several heterogeneous photocatalysts, including the previously reported Zinc Indium sulfides, were investigated for the conversion of aromatic alcohols to C–C coupling products under the reaction conditions used in this study (Table 1) [36–40]. The optimized ZnIn sulfide (entry 2, Table 1) showed an overall conversion yield of < 80% despite its high selectivity for the C–C coupling products. Ag_2S(5%)@CdS exhibited the highest conversion yield and C–C coupling product selectivity among all the photocatalysts investigated.

The applicability of Au_2S(5%)@CdS and Ag_2S(5%)@CdS to the photocatalytic conversion of other substituted benzyl alcohols with -OCH_3, -CH_3 and -F as the substrates was verified under identical reaction conditions. As shown in Table S2, Au_2S(5%)@CdS and Ag_2S(5%)@CdS exhibited a conversion yield of >80% and a high selectivity of >85% toward the benzaldehyde species and C–C coupling products, respectively. In particular, the preservation of the selectivity of Ag_2S(5%)@CdS toward the C–C coupling products can be attributed to the stability of the ketyl radical species generated during the photooxidation reaction and the increased probability of coupling the ketyl radical species.

3.4. Control experiments for photoredox mechanism investigation

The radical characteristics of the photocatalytic conversion for C–C coupling over Ag_2S(5%)@CdS were evaluated by investigating the effect of a radical scavenger, 2,2,6,6-tetramethylpiperidinyloxy (TEMPO) (for trapping the photogenerated electrons), on the photoconversion mechanisms [48]. In the presence of TEMPO, the photocatalytic conversion yield of Ag_2S(5%)@CdS was reduced to 5% and, surprisingly, the converted main product was benzaldehyde, not the C–C coupling product. This occurred because the photoredox ability of the catalyst was reduced by photogenerated electron trapping, and the oxidation reaction of benzyl alcohol became dominant (Fig. S9). Moreover, electron paramagnetic resonance was employed for monitoring the radical species generated using the radical-trapping reagent, 5,5-dimethyl-1-pyrrolidinyloxy (DMPO), during the photocatalytic reaction [48]. As shown in Fig. S10, electron spin resonance peaks corresponding to the carbon–DMPO radical species were generated during the photocatalytic reaction when the Ag_2S(5%)@CdS NPs were used. These results clearly indicate that the photocatalytic conversion of benzyl alcohol over the Ag_2S(5%)@CdS and Au_2S(5%)@CdS NPs proceeded via a radical mechanism.

Photoluminescence (PL) studies were carried out to investigate the transitions of the photogenerated electrons in the pristine CdS, Ag_2S(5%)@CdS, and Au_2S(5%)@CdS NPs; the results are shown in Fig. S11. The PL emission spectra of the photocatalysts were recorded over the wavelength range of 470−50 nm at an excitation wavelength of 410 nm. The intensities of the emission bands of the Ag_2S(5%)@CdS and Au_2S(5%)@CdS NPs decreased drastically compared to that of the emission band of the pristine CdS NPs, indicating the occurrence of the transfer of the photogenerated electrons and holes from CdS to Ag_2S and Au_2S in the composite systems [62,63]. Moreover, the time-resolved fluorescence measurement data for CdS, Ag_2S(5%)@CdS, and Au_2S(5%)@CdS were obtained by time-correlated single photon counting (TCSPC) analysis (Fig. S12 and Table S3). These results corroborated with the PL spectral observations. The average PL decay lifetimes of Ag_2S(5%)@CdS and Au_2S(5%)@CdS were 3.7 and 2.7 ns, respectively, which were lower than that of CdS (5.3 ns). This decrease in the photogenerated charge carrier lifetimes can be attributed to the enhanced charge transfer between CdS and Ag_2S or Au_2S in the composite CdS system.

Consequently, for assessing the high conversion yield of Ag_2S(5%)@CdS and Au_2S(5%)@CdS, the transient photocurrent densities of the pristine CdS, Ag_2S(5%)@CdS and Au_2S(5%)@CdS NPs upon regularly chopped blue LED irradiation were measured (Fig. S13(a–c)). Upon the addition of benzyl alcohol (as a substrate) to the electrolyte, the transient photocurrent densities of Ag_2S(5%)@CdS and Au_2S(5%)@CdS drastically increased compared to those of systems wherein benzyl alcohol was not added. In contrast, the difference in the photocurrent densities of pristine CdS in the presence and absence of benzyl alcohol is negligible. This indicated that Ag_2S(5%)@CdS and Au_2S(5%)@CdS efficiently photocatalyzed the conversion of benzyl alcohol because Ag_2S and Au_2S as a co-catalyst can inhibit the recombination of photoexcited electron–hole pairs in Ag_2S(5%)@CdS and Au_2S(5%)@CdS in the presence of benzyl alcohol. Additionally, electrochemical impedance spectroscopy (EIS) was performed to investigate the charge transport between the sample and electrolyte. As displayed Fig. S13(d), both Ag_2S(5%)@CdS and Au_2S(5%)@CdS show a more high-frequency depressed semicircle than pristine CdS, confirming more efficient transfer of the photogenerated electron–hole pairs in Ag_2S(5%)@CdS and Au_2S(5%)@CdS than that in pristine CdS.

Table 1
Photoconversion of benzyl alcohol over various composites of ZnIn sulfides.

Entry	Catalyst	Conversion yield (%)	Product yield (%)		
		Benzaldehyde	C–C coupling product		
			Benzoin	Hydrobenzoin	Deoxybenzoin
1	$Zn_{0.2}In_2S_{3.2}$[a]	50	13	12	24	1
2	$Zn_{0.6}In_2S_{3.6}$[a]	74	–	–	71	3
3	$ZnIn_2S_4$[a]	47	–	–	44	2
4	$ZnIn_2S_4$[b]	22	8	–	13	–
5	$Zn_2In_2S_5$[b]	31	10	1	19	–
6	$Zn_3In_2S_6$[b]	25	4	–	19	–
7	$Zn_4In_2S_7$[b]	28	2	10	10	1
8	$Zn_5In_2S_8$[b]	41	9	2	30	–
9	$Zn_6In_2S_9$[b]	24	4	–	19	–
10	Ag_2S(5%)@CdS	100	3	–	–	97

[a]Ref. [37], [b]Ref. [38], Reaction conditions: 0.1 mmol of benzyl alcohol, 5 mg of the catalyst, 1.0 mL of CH_3CN, 4 h, Ar atmosphere, 6 W blue LEDs (445 nm) at ~35 °C.

3.5. Revealing the role of Ag2S and Au_2S from changes in the electronic structure

The energy diagrams of the pristine CdS, Ag_2S(5%)@CdS, and Au_2S (5%)@CdS NPs could be constructed by setting their bandgaps because the ion exchange of the CdS NPs with Ag^+ and Au^+ did not change their bandgap (~2.4 eV). To determine the Fermi levels of the pristine CdS, Ag_2S(5%)@CdS, and Au_2S(5%)@CdS NPs, UPS was carried out; the results are shown in Fig. 5. The UP spectra revealed that the Fermi level of the pristine CdS NPs changed after the cation exchange process (in the cases of the Ag_2S(5%)@CdS and Au_2S(5%)@CdS NPs). The Fermi level of the pristine CdS NPs was located at 2.21 eV above the middle bandgap, indicating that the NPs showed typical n-type characteristics [42]. Remarkably, the Fermi level of Ag_2S(5%)@CdS shifted upward by 0.14 eV (2.35 eV) to just below the estimated conduction band (CB) because the bandgap energy of Ag_2S was close to the CB of CdS. The growth of Ag_2S on CdS led to the photoinduced transfer of electrons within the CB of CdS to Ag_2S, allowing the reduction of H^+ to H_2 and the reductive dehydration of the hydrobenzoin ketyl radical to deoxybenzoin as seen Fig. S14. This can be attributed to the accelerated photoredox reaction of benzyl alcohol in the presence of Ag_2S(5%)@CdS with high deoxybenzoin selectivity. This is consistent with the photocatalytic measurement results. In contrast, the Fermi level of the Au_2S (5%)@CdS NPs shifted downward (0.15 eV) closer to the top of the valence band (VB) of CdS. The growth of Au_2S on CdS led to the photoinduced transfer of h^+ within the VB of CdS to Au_2S. This can be attributed to the enhanced oxidation ability of Au_2S(5%)@CdS toward benzyl alcohol, which is consistent with the photocatalytic measurement results.

To elucidate the feasibility of the interfacial photogenerated electron–hole transfer in Ag_2S(5%)@CdS and Au_2S(5%)@CdS and to confirm the existence of the two proposed photocatalytic reaction routes, in situ HR-XPS analysis was carried out under light radiation (Fig. 6) [49,50]. In the absence of light radiation, the HR-XPS profile of the pristine CdS NPs showed two typical characteristic peaks at the binding energies of 404.8 and 411.6 eV corresponding to Cd $3d_{5/2}$ and Cd $3d_{3/2}$, respectively. The origin of these peaks can be attributed to the Cd^{2+} ions present in CdS [51]. Interestingly, the HR-XPS Cd 3d profiles of Ag_2S(5%)@CdS and Au_2S(5%)@CdS showed two additional doublets at 406.0/412.8 eV (1.2 eV higher) and 403.7/410.5 eV (1.1 eV lower), respectively (Fig. 6(a)). The HR-XPS profile of pristine CdS showed two S 2p peaks at 161.1 and 162.3 eV corresponding to S $2p_{3/2}$ and $2p_{1/2}$, respectively [51]. Similar to the Cd 3d HR-XPS profiles, the S 2p profiles of Ag_2S(5%)@CdS and Au_2S(5%)@CdS showed two doublets at 162.4/163.6 eV and 162.0/163.1 eV, respectively [52,53]. These binding energies are higher than those of the S 2p peaks of CdS, as shown in Fig. 6(b). These results confirm the interaction between CdS and Ag_2S or Au_2S in the hybrid composites, which contributed to the construction of well-defined Ag_2S(5%)@CdS and Au_2S(5%)@CdS heterostructures.

In addition, Ag_2S(5%)@CdS showed two distinct Ag^+ peaks at 374.2 and 368.3 eV corresponding to Ag $3d_{5/2}$ and Ag $3d_{3/2}$, respectively (Fig. 6(c)) [49]. In contrast, Au_2S(5%)@CdS showed two Au^+ peaks at 86.2 and 89.8 eV corresponding to Au $4f_{7/2}$ and Au $4f_{5/2}$, respectively (Fig. 6(d)) [50]. The HR-XPS results for the oxidation states of Ag^+ and Au^+ confirmed the successful formation of the Ag_2S@CdS and Au_2S@CdS heterostructures.

The interfacial photogenerated electron–hole transfer in the Ag_2S (5%)@CdS and Au_2S(5%)@CdS photocatalysts was further corroborated by performing in situ XPS measurements under blue LED (445 nm) radiation. Interestingly, when Ag_2S(5%)@CdS was irradiated, the binding energies of the Cd 3d and S 2p peaks increased by 0.2 eV and decreased by 0.4 eV, respectively, as compared to those of the peaks observed in the absence of radiation, as shown in Fig. 6. Simultaneously, the binding energies of the Ag 3d peaks decreased by approximately 0.4 eV as compared to those of the peaks observed in the absence of radiation. This result suggests that the electron density of Ag_2S increased, while that of Cd^{2+} decreased in Ag_2S(5%)@CdS during the photoexcitation process. These changes in the electron densities of Ag_2S and Cd^{2+} provide direct evidence for the transfer of the photogenerated electrons in CdS to Ag_2S upon LED irradiation, as shown in Fig. 6(d). The accumulation of the photogenerated electrons on Ag_2S enhanced the photoredox ability of Ag_2S(5%)@CdS, which is in good agreement with the improvement in the photocatalytic performance of Ag_2S(5%)@CdS indicated in Scheme 1.

In contrast, Au_2S(5%)@CdS showed an opposite trend. Upon irradiation, the binding energies of the Cd $3d_{5/2}$/$3d_3$/2 and S $2p_{3/2}$/$2p_{1/2}$

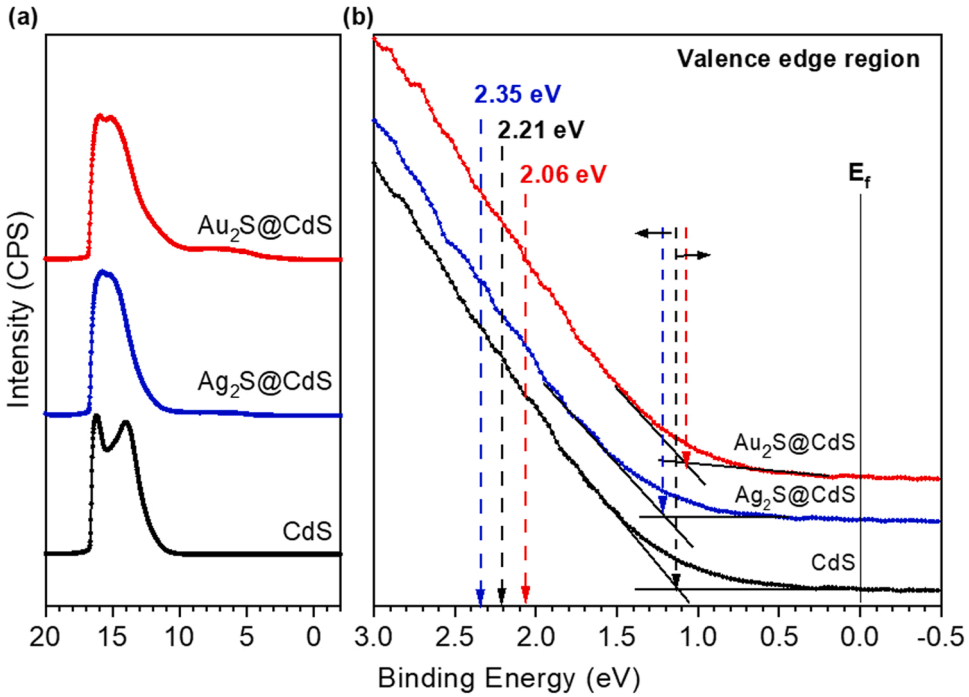

Fig. 5. UP spectra (a) and valence edge regions (b) of the pristine CdS, Au_2S(5%)@CdS and Ag_2S(5%)CdS.

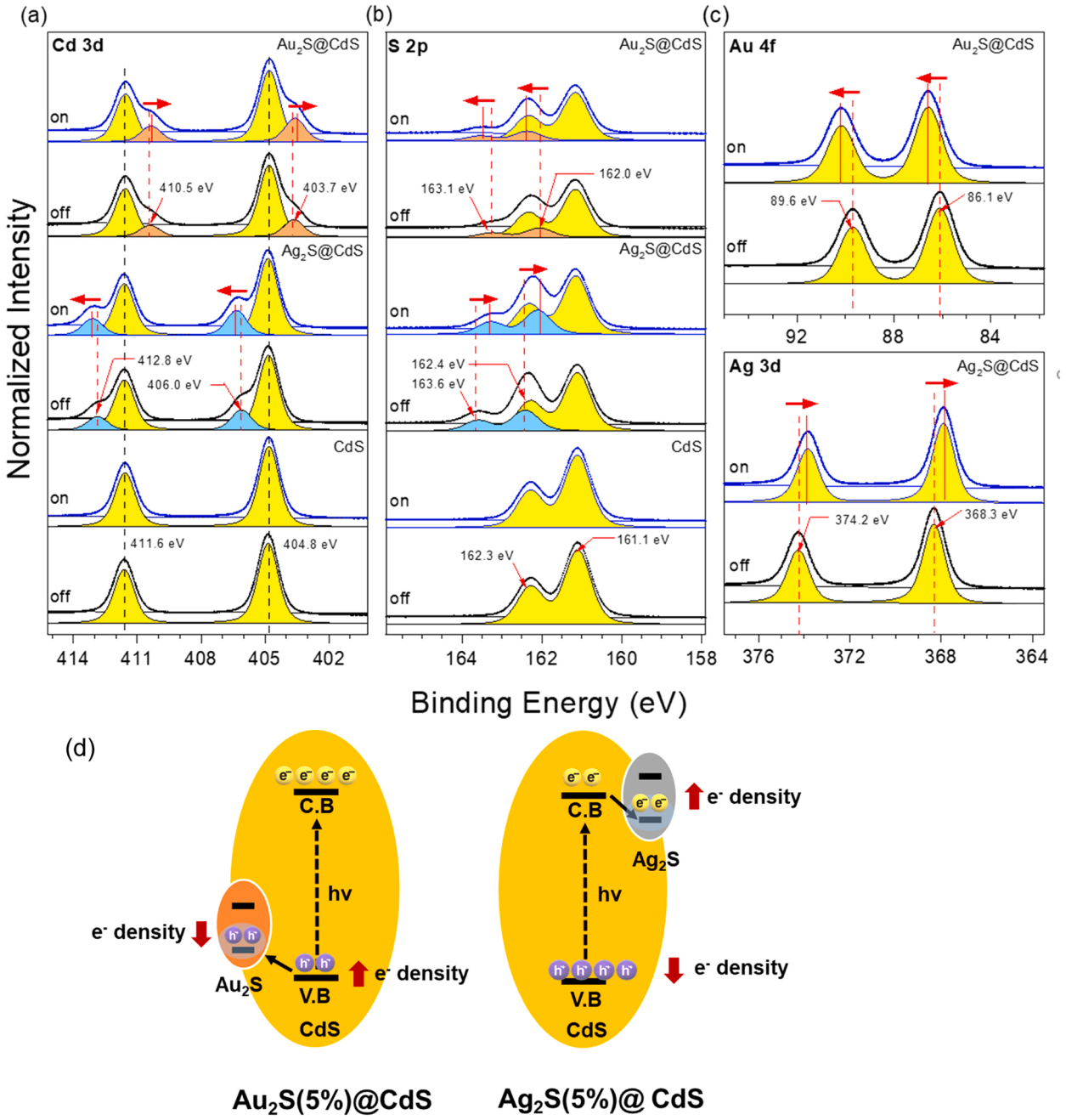

Fig. 6. High-resolution XPS Cd 3d(a), S 2p (b), Au 4f (c), and Ag 3d core-level profiles. Schematic illustration of the transfer of the photogenerated electrons and holes in Au_2S(5%)@CdS and Ag_2S(5%)CdS (d).

peaks decreased by 0.1 eV and increased by 0.4 eV, respectively, as compared to those obtained in the absence of radiation. Moreover, the binding energies of the Au 4 $f_{7/2}$ and Au 4 $f_{5/2}$ peaks increased by approximately 0.2 eV as compared to those obtained in the absence of radiation. This indicates that the electron density of Au_2S decreased, while that of Cd^{2+} increased during the photoexcitation process. The photogenerated holes in the VB of CdS transferred to Au_2S. The accumulation of the photogenerated holes in Au_2S enhanced the photooxidation ability of Au_2S(5%)@CdS. This observation is in good agreement with the improvement in the photocatalytic performance of Au_2S(5%)@CdS toward benzaldehyde production.

4. Conclusion

We proposed a visible-light-driven photocatalytic approach for the production of benzaldehyde or deoxybenzoin as the C–C coupling product with a high conversion yield from benzyl alcohol. We modified CdS NPs with Au_2S and Ag_2S to form heterogeneous photocatalysts via the ion exchange process. By changing the exchange cation (Ag^+ or Au^+), the main product of the photocatalytic conversion of benzyl alcohol could be changed. The Au_2S(5%)@CdS NPs produced benzaldehyde as the main product because of the transfer of the photogenerated holes between CdS and Au_2S, which led to an improvement in the photooxidation ability of the NPs. In contrast, when Ag_2S(5%)@CdS was used, deoxybenzoin was formed as the C–C coupling product because of the consecutive photooxidation for the formation of ketyl radicals and the photoreductive dehydration of hydrobenzoin by the coupling of the ketyl radicals via the transfer of the photogenerated electrons between CdS and Ag_2S. The results demonstrated the feasibility of the formation of heterostructure composites via a simple ion

exchange process and the formation of the desired product during the photooxidation of aromatic alcohols by simply changing the ion exchange species in the photocatalyst. Therefore, this study provides a novel strategy for the preparation of heterostructure composites comprising appropriate cocatalysts for the conversion of alcohols to useful compounds through the C–C coupling process.

CRediT authorship contribution statement

Sung-Gyu Lee: Methodology, Data curation, Formal analysis. **Myung Jong Kang:** Data curation, Formal analysis. **Myeongkee Park:** Data curation, Formal analysis. **Ki-jeong Kim:** Data curation, Formal analysis. **Hangil Lee:** Data curation, Formal analysis, Funding acquisition, Resources. **Hyun Sung Kim:** Conception, Writing – review & editing, Funding acquisition, Resources.

Declaration of Competing Interest

The authors declare that they have no known competing financial interests or personal relationships that could have appeared to influence the work reported in this paper.

Acknowledgement

This work was supported by the National Research Foundation of Korea (NRF), Republic of Korea grant funded by the Korea government (MSIT) (2020R1A2C1010725). H. Lee thanks the National Research Foundation of Korea (NRF) funded by the Korea government (MSIT) (2021R1A2C2007992). This work was also partly supported by Ministry of Science and ICT (MSIT) and the Pohang Accelerator Laboratory (PAL), Republic of Korea.

Appendix A. Supporting information

Supplementary data associated with this article can be found in the online version at doi:10.1016/j.apcatb.2021.120967.

References

[1] C.Y. Toe, C. Tsounis, J. Zhang, H. Masood, D. Gunawan, J. Scott, R. Amal, Advancing photoreforming of organics: Highlights on photocatalyst and system designs for selective oxidation reactions, Energy Environ. Sci. 14 (2021) 1140–1175.
[2] J. Xie, H. Jin, A.S.K. Hashmi, The recent achievements of redox-neutral radical C-C cross-coupling enabled by visible-light, Chem. Soc. Rev. 46 (2017) 5193–5203.
[3] J.Y. Li, Y.H. Li, M.Y. Qi, Q. Lin, Z.R. Tang, Y.J. Xu, Selective organic transformations over cadmium sulfide-based photocatalysts, ACS Catal. 10 (2020) 6262–6280.
[4] J. Kiwi, S. Rtimi, Insight into the interaction of magnetic photocatalysts with the incoming light accelerating bacterial inactivation and environmental cleaning, Appl. Catal. B Environ. 281 (2021), 119420.
[5] J.-H. Tang, Y. Sun, Visible-light-driven organic transformations integrated with H2 production on semiconductors, Mater. Adv. 1 (2020) 2155–2162.
[6] Kirk-Othmer, Kirk-Othmer Encyclopedia of Chemical Technology, fourth ed., Wiley, New York, 1993.
[7] J.A.B. Satrio, L.K. Doraiswamy, Production of benzaldehyde: a case study in a possible industrial application of phase-transfer catalysis, Chem. Eng. J. 82 (2001) 43–56.
[8] G.D. McAllister, A.F. Parsons, Going green in process chemistry: optimizing an asymmetric oxidation reaction to synthesize the antiulcer drug esomeprazole, J. Chem. Educ. 96 (2019) 2617–2621.
[9] A. Alan I, Process of maufacturing bezaldehyde, 1919.
[10] J.E. Mcmurry, V.I. Keto, E. Couplings, Carbonyl-coupling reactions, Chem. Rev. 89 (1989) 1513–1524.
[11] H.C. Kolb, M.S. VanNieuwenhze, K. Barry Sharpless , Catalytic asymmetric dihydroxylation, Chem. Rev. 94 (199) 2483–2547.
[12] H.Q. Li, Y. Luo, R. Song, Z.L. Li, T. Yan, H.L. Zhu, Design, synthesis, and immunosuppressive activity of new deoxybenzoin derivatives, ChemMedChem 5 (2010) 1117–1122.
[13] X. Hu, Y. Wang, J. Yu, J. Zhu, Z. Hu, Synthesis of a deoxybenzoin derivative and its use as a flame retardant in poly(trimethylene terephthalate), J. Appl. Polym. Sci. 135 (2018) 1–8.
[14] K. Okano, Tetrahedron report number 935: Synthesis and application of chiral hydrobenzoin, Tetrahedron 67 (2011) 2483–2512.
[15] C.F.H. Allen, W.E. Barker, Desoxybenzoin, Org. Synth. 2 (1943) 156.
[16] M. Ghahremani, R. Ciriminna, V. Pandarus, A. Scurria, V. La Parola, F. Giordano, G. Avellone, F. Béland, B. Karimi, M. Pagliaro, Green and direct synthesis of benzaldehyde and benzyl benzoate in one pot, ACS Sustain. Chem. Eng. 6 (2018) 15441–15446.
[17] L. Wang, Z. Huang, S. Xie, Q. Zhang, H. Wang, Y. Wang, Photocatalytic C−H activation and C−C coupling of monohydric alcohols, Catal. Commun. 153 (2021), 106300.
[18] M.A. Fox, Organic heterogeneous photocatalysis: chemical conversions sensitized by irradiated semiconductors, Acc. Chem. Res. 16 (1983) 314–321.
[19] V. Augugliaro, L. Palmisano, Green oxidation of alcohols to carbonyl compounds by heterogeneous photocatalysis, ChemSusChem 3 (2010) 1135–1138.
[20] D. Friedmann, A. Hakki, H. Kim, W. Choi, D. Bahnemann, Heterogeneous photocatalytic organic synthesis: State-of-the-art and future perspectives, Green Chem. 18 (2016) 5391–5411.
[21] L. Chen, J. Tang, L.N. Song, P. Chen, J. He, C.T. Au, S.F. Yin, Heterogeneous photocatalysis for selective oxidation of alcohols and hydrocarbons, Appl. Catal. B Environ. 242 (2019) 379–388.
[22] J. Pan, B. Wang, J. Wang, H. Ding, W. Zhou, X. Liu, J. Zhang, S. Shen, J. Guo, L. Chen, C. Au, L. Jiang, S.F. Yin, Activity and stability boosting of an oxygen-vacancy-rich BiVO4 photoanode by NiFe-MOFs thin layer for water oxidation, Angew. Chem. 133 (2021) 1453–1460.
[23] T. Mitkina, C. Stanglmair, W. Setzer, M. Gruber, H. Kisch, B. König, Visible light mediated homo- and heterocoupling of benzyl alcohols and benzyl amines on polycrystalline cadmium sulfide, Org. Biomol. Chem. 10 (2012) 3556–3561.
[24] S. Wang, B. Zhu, M. Liu, L. Zhang, J. Yu, M. Zhou, Direct Z-scheme ZnO/CdS hierarchical photocatalyst for enhanced photocatalytic H2-production activity, Appl. Catal. B Environ. 243 (2019) 19–26.
[25] C. Jiang, H. Wang, Y. Wang, H. Ji, All solid-state Z-scheme CeO2/ZnIn2S4 hybrid for the photocatalytic selective oxidation of aromatic alcohols coupled with hydrogen evolution, Appl. Catal. B Environ. 277 (2020), 119235.
[26] Y. Zou, Y. Hu, A. Uhrich, Z. Shen, B. Peng, Z. Ji, M. Muhler, G. Zhao, X. Wang, X. Xu, Steering accessible oxygen vacancies for alcohol oxidation over defective Nb2O5 under visible light illumination, Appl. Catal. B Environ. 298 (2021), 120584.
[27] Z. Sun, X. Yang, X.F. Yu, L. Xia, Y. Peng, Z. Li, Y. Zhang, J. Cheng, K. Zhang, J. Yu, Surface oxygen vacancies of Pd/Bi2MoO6-x acts as "Electron Bridge" to promote photocatalytic selective oxidation of alcohol, Appl. Catal. B Environ. 285 (2021), 119790.
[28] S. Meng, X. Ning, S. Chang, X. Fu, X. Ye, S. Chen, Simultaneous dehydrogenation and hydrogenolysis of aromatic alcohols in one reaction system via visible-light-driven heterogeneous photocatalysis, J. Catal. 357 (2018) 247–256.
[29] C. Han, Z.R. Tang, J. Liu, S. Jin, Y.J. Xu, Efficient photoredox conversion of alcohol to aldehyde and H2 by heterointerface engineering of bimetal-semiconductor hybrids, Chem. Sci. 10 (2019) 3514–3522.
[30] C. Ling, X. Ye, J. Zhang, J. Zhang, S. Zhang, S. Meng, X. Fu, S. Chen, Solvothermal synthesis of CdIn2S4 photocatalyst for selective photosynthesis of organic aromatic compounds under visible light, Sci. Rep. 7 (27) (2017) 1–16.
[31] Z. Yang, X. Xia, W. Yang, L. wang, Y. Liu, Photothermal effect and continuous hot electrons injection synergistically induced enhanced molecular oxygen activation for efficient selective oxidation of benzyl alcohol over plasmonic W18O49/ZnIn2S4 photocatalyst, Appl. Catal. B Environ. 299 (2021), 120675.
[32] Z. Chai, T.T. Zeng, Q. Li, L.Q. Lu, W.J. Xiao, D. Xu, Efficient visible light-driven splitting of alcohols into hydrogen and corresponding carbonyl compounds over a Ni-modified CdS photocatalyst, J. Am. Chem. Soc. 138 (2016) 10128–10131.
[33] M. Sahoo, S. Mansingh, K.M. Parida, A bimetallic Au-Ag nanoalloy mounted LDH/RGO nanocomposite: a promising catalyst effective towards a coupled system for the photoredox reactions converting benzyl alcohol to benzaldehyde and nitrobenzene to aniline under visible light, J. Mater. Chem. A 7 (2019) 7614–7627.
[34] L. Xiao, Q. Zhang, P. Chen, L. Chen, F. Ding, J. Tang, Y.J. Li, C.T. Au, S.F. Yin, Copper-mediated metal-organic framework as efficient photocatalyst for the partial oxidation of aromatic alcohols under visible-light irradiation: synergism of plasmonic effect and schottky junction, Appl. Catal. B Environ. 248 (2019) 380–387.
[35] J. He, L. Chen, D. Ding, Y.K. Yang, C.T. Au, S.F. Yin, Facile fabrication of novel Cd3(C3N3 S3)2/CdS porous composites and their photocatalytic performance for toluene selective oxidation under visible light irradiation, Appl. Catal. B Environ. 233 (2018) 243–249.
[36] Y. Song, J. Zhang, X. Dong, H. Li, A review and recent developments in full-spectrum photocatalysis using ZnIn2S4-based photocatalysts, Energy Technol. 9 (2021) 1–29.
[37] N. Luo, T. Hou, S. Liu, B. Zeng, J. Lu, J. Zhang, H. Li, F. Wang, Photocatalytic coproduction of deoxybenzoin and H2 through tandem redox reactions, ACS Catal. 10 (2020) 762–769.
[38] Q. Lin, Y.H. Li, M.Y. Qi, J.Y. Li, Z.R. Tang, M. Anpo, Y.M.A. Yamada, Y.J. Xu, Photoredox dual reaction for selective alcohol oxidation and hydrogen evolution over nickel surface-modified ZnIn2S4, Appl. Catal. B Environ. 271 (2020), 118946.
[39] G. Han, X. Liu, Z. Cao, Y. Sun, Photocatalytic pinacol C-C coupling and jet fuel precursor production on ZnIn2S4 nanosheets, ACS Catal. 10 (2020) 9346–9355.
[40] M.Y. Qi, Y.H. Li, M. Anpo, Z.R. Tang, Y.J. Xu, Efficient photoredox-mediated C-C coupling organic synthesis and hydrogen production over engineered semiconductor quantum dots, ACS Catal. 10 (2020) 14327–14335.
[41] K.P. McClelland, E.A. Weiss, Selective photocatalytic oxidation of benzyl alcohol to benzaldehyde or C-C coupled products by visible-light-absorbing quantum dots, ACS Appl. Energy Mater. 2 (2019) 92–96.

[42] Y.J. Yuan, D. Chen, Z.T. Yu, Z.G. Zou, Cadmium sulfide-based nanomaterials for photocatalytic hydrogen production, J. Mater. Chem. A 6 (2018) 11606–11630.
[43] X. Sun, D. Jiang, L. Zhang, W. Wang, Alkaline modified g-C3N4 photocatalyst for high selective oxide coupling of benzyl alcohol to benzoin, Appl. Catal. B Environ. 220 (2018) 553–560.
[44] B. Sadtler, D.O. Demchenko, H. Zheng, S.M. Hughes, M.G. Merkle, U. Dahmen, L. W. Wang, A.P. Alivisatos, Selective facet reactivity during cation exchange in cadmium sulfide nanorods, J. Am. Chem. Soc. 131 (2009) 5285–5293.
[45] A.C. Poulose, S. Veeranarayanan, Y. Yoshida, T. Maekawa, D.S. Kumar, Rapid synthesis of triangular CdS nanocrystals without any trap emission, J. Nanopart. Res. 14 (789) (2012) 1–10.
[46] S. Xiong, B. Xi, K. Zhang, Y. Chen, J. Jiang, J. Hu, H.C. Zeng, Ag nanoprisms with Ag2S attachment, Sci. Rep. 3 (2177) (2013) 1–9.
[47] H. Zhu, T. Cai, Y. Yuan, X. Wang, Y. Nagaoka, J. Zhao, Z. Liu, R. Li, O. Chen, Pressure-induced transformations of three-component heterostructural nanocrystals with CdS-Au2S Janus nanoparticles as hosts and small Au nanoparticles as satellites, ACS Appl. Nano Mater. 2 (2019) 6804–6808.
[48] J.T. Schneider, D.S. Firak, R.R. Ribeiro, P. Peralta-Zamora, Use of scavenger agents in heterogeneous photocatalysis: truths, half-truths, and misinterpretations, Phys. Chem. Chem. Phys. 22 (2020) 15723–15733.
[49] B. He, C. Bie, X. Fei, B. Cheng, J. Yu, W. Ho, A.A. Al-Ghamdi, S. Wageh, Enhancement in the photocatalytic H2 production activity of CdS NRs by Ag2S and NiS dual cocatalysts, Appl. Catal. B Environ. 288 (2021), 119994.
[50] J. Low, B. Dai, T. Tong, C. Jiang, J. Yu, In situ irradiated X-Ray photoelectron spectroscopy investigation on a direct Z-scheme TiO2/CdS composite film photocatalyst, Adv. Mater. 31 (2019) 1–5.
[51] T. Abe, Y. Kashiwaba, M. Baba, J. Imai, H. Sasaki, XPS analysis of p-type Cu-doped CdS thin films, Appl. Surf. Sci. 175-176 (2001) 549–554.
[52] T.Y. Liang, S.J. Chan, A.S. Patra, P.L. Hsieh, Y.A. Chen, H.H. Ma, M.H. Huang, Inactive Cu2O cubes become highly photocatalytically active with Ag2S deposition, ACS Appl. Mater. Interfaces 13 (2021) 11515–11523.
[53] B. Gadgil, P. Damlin, A. Viinikanoja, M. Heinonen, C. Kvarnström, One-pot synthesis of an Au/Au2S viologen hybrid nanocomposite for efficient catalytic applications, J. Mater. Chem. A 3 (2015) 9731–9737.